ELSEVIER

Optical Materials 19 (2002) 403–413

OPTICAL Materials

www.elsevier.com/locate/optmat

Passively Q-switched diode-pumped Yb:YAG laser using Cr^{4+}-doped garnets

Y. Kalisky [a,*], C. Labbe [a], K. Waichman [a,b], L. Kravchik [a], U. Rachum [a], P. Deng [c], J. Xu [c], J. Dong [c], W. Chen [c]

[a] *"Arava" Laser Laboratory, Rotem Industrial Park, D.N. Arava, Mishor Yamin 86800, Israel*
[b] *Laser Department, NuclearResearch Centre Negev, P.O. Box 9001, Beer Sheva 89140, Israel*
[c] *Crystal Laboratory, Shanghai Institute of Optics and Fine Mechanics, Chinese Academy of Sciences, P.O. Box 800-216, Shanghai 201800, China*

Received 29 June 2001; received in revised form 15 October 2001; accepted 26 November 2001

Abstract

We investigate the repetitive modulation in the kHz frequency domain of a passively Q-switched, diode-pumped Yb:YAG laser, by Cr^{4+}:YAG, Cr^{4+}:LuAG, and Cr^{4+}:GSGG saturable absorbers. The results presented here are focused towards the design of a passively Q-switched Yb:YAG microlaser. The free-running performance of both rod and a disk Yb:YAG is characterized and experimental parameters such as gain and loss are evaluated. These values, together with the value of the stimulated emission cross-section, e.g. $\sigma_{em} = 3.3 \times 10^{-20}$ cm^2 were found to fit between our experimental results and an existing numerical model which relates the experimental and physical parameters to the minimal threshold pumping power. Q-switched pulses with maximum peak power of ≈10.4 kW, with energy of ≈0.5 mJ/pulse, were extracted with 30% extraction efficiency.

Keywords: Diode pumped lasers; Passive Q-switching; Yb:YAG laser

1. Introduction

Passively Q-switched, diode pumped solid state lasers are currently being used as miniature or microlasers capable of delivering high peak output power at high repetition rates and short nanosecond (ns) temporal pulsewidth. These lasers are of great interest due to their potential applications in micromachining, remote sensing, target ranging, and microsurgery. Most commonly, systems presently used are based on Nd:YAG or Nd:YVO_4 lasers, passively Q-switched by Cr^{4+}:YAG, where the unique characteristics of Cr^{4+} garnets as saturabale absorbers are utilized [1].

Similarly to the Nd^{3+}/Cr^{4+}:YAG system, it is anticipated that the Yb^{3+}/Cr^{4+} laser system will posses significant advantages related to microlasers and their applications. During the last several years there are convincing indications pertaining the Yb^{3+}-based diode-pumped lasers and their possibility to replace the currently used Nd^{3+}-based systems, in particular the diode-pumped systems.

* Corresponding author. Tel.: +972-7-655-6301; fax: +972-7-655-5984.
E-mail address: ykalisky@actcom.co.il (Y. Kalisky).

0925-3467/02/$ - see front matter
PII: S0925-3467(02)00003-4

Solid state lasers based on Yb^{3+} doped solid hosts emit coherent radiation peaking at 1030 nm via $^2F_{5/2}(A_1) \rightarrow {}^2F_{7/2}(Z_3)$, levels, where A_1 and Z_3 are the J-Stark components located at 10,327 and 612 cm^{-1}, respectively [2]. Yb-based solid-state lasers have several advantages over Nd-doped lasers. The advantages of Yb laser can be summarized as follows:

- Low quantum defect e.g. 91% quantum efficiency, hence low fractional heating (<11% as compared to 37–43% in Nd^{3+}:YAG) [3], and smaller thermal load on the crystal.
- Broad absorption bandwidth of about 10 nm and 940 nm ($^2F_{7/2} \rightarrow {}^2F_{5/2}$), that implies more flexibility on the pumping diode wavelength control within the absorption band of the gain medium, and on the diode temperature. (This absorption bandwidth is five times broader than the 808-nm absorption transition in Nd:YAG.)
- Broad emission bandwidth which results in tunability and the ability to generate short pulses.
- High doping levels—up to 20 at.% and even higher levels, without concentration quenching of the excited states.
- Due to the simple $4f^{13}$ electronic configuration of Yb^{3+} ion, there are no relevant higher lying excited states, and therefore, there is no excited state absorption, upconversion phenomena, nonradiative processes among excited states, or quenching of excited state luminescence.
- Pumping wavelengths of 940 or 970 nm—utilization of the reliable Al-free InGaAs diode lasers
- Yb is capable of energy storage due to its long lifetime—in the 0.95–1.2 ms temporal domain, and the low emission cross-section.
- Finally, there is significant advantage in using the YAG as laser host since both Yb and Nd doped YAG posses robust thermal and mechanical properties of the hosting YAG.

The main physical and optical characteristics of Yb^{3+}:YAG are summarized in Table 1.

The main disadvantage of Yb doped host is its quasi-three-level nature due to the thermal population of the highest J splitting of the $^4F_{7/2}$ lower terminating lasing level, which is about 612 cm^{-1} above the ground level. This thermal population has deleterious effects of resonant re-absorption of the laser emission from the ground terminal Stark state, which is thermally populated at 300 K by about 5% of the $^4F_{7/2}$ population. Therefore, it is difficult to obtain population inversion at room temperature, and therefore, the lasing threshold is high and its efficiency is consequently low. Efficient population inversion is achieved by either pumping at high pump power densities at 300 K (1.5–10 kW/cm^2) [4], or by depopulation of the highest Stark components. The latter option is achieved by

Table 1
Main physical characteristics of Yb:YAG crystal

Characteristics	Nomenclature	Value	Reference
σ_p, cm^2 @ 940 nm	Absorption cross-section	7.4×10^{-21}	[16]
		7.7×10^{-21}	[17]
σ_{em}, cm^2 @ 1030 nm	Emission cross-section	2.3×10^{-20}	[13]
		3.3×10^{-20}	[18]
κ, W/m K @ 300 K	Thermal conductivity	13	
dn/dT	Change of refraction index with temperature	8.9×10^{-6}	[19]
		7.3×10^{-6}	[7,12]
		9.86×10^{-6}	[20]
τ_{fl}, ms @ 300 K	Fluorescence lifetime	0.951	[21]
λ_p, nm	Pumping wavelength	940	
λ_{em}, nm	Emission wavelength	1030	
α, cm^{-1}	Absorption coefficient (8 at.%)	8	Measured, this work
	Absorption coefficient (10 at.%)	10	
η_{th}, %	Fractional thermal load	11	[3]
C_{Yb}, ions/cm^3	Ionic concentration	1.38×10^{20} (1.0 at.%)	

cooling down the system to low temperatures, where only the lowest Stark levels are thermally populated.

For several applications, mainly industrial, Q-switched nanosecond pulses are the preferred choice over the high peak power, sub picosecond mode-locked Yb:YAG laser system [5]. It is therefore necessary to optimize the conditions, which allow the passively Q-switched operation of Yb:YAG laser towards applications that require mid-levels of average power or alternatively, medium peak power level at 300 K, utilizing a compact and simple system.

The ytterbium laser is currently regarded as a suitable candidate to generate pulses having relatively high peak power, due to the long lifetime of the excited level $^2F_{5/2}$ of Yb^{3+} ion. This characteristics, coupled with the ability to obtain high Yb^{3+} doping levels (up to 20 at.% without concentration quenching), make the ytterbium doped solids an ideal candidate as a microlaser in the 1030–1050 nm spectral range. This laser is passively Q-switched by saturable absorbers such as Cr^{4+}:YAG and other quadrivalent chromium doped garnets, yielding repetitive modulation and high peak power pulses.

In the present paper, we investigate the optimal parameters of an efficient operation of a microlaser based on a passively Q-switched diode-pumped Yb:YAG laser, using several Cr^{4+}-doped garnets as saturable absorbers.

2. Experimental

The laser experimental set-up is presented in Fig. 1. Two types of Yb:YAG crystals were used to study the repetitive modulation and passively Q-switching of Yb laser. The Yb:YAG laser rod, (sample #1) supplied by VLOC (FL, USA), was $\phi = 2$ mm in diameter and $l = 4$ mm in length, and was doped with 10 at.% of Yb^{3+}. The Yb-doped disk YAG crystal-denoted as sample #2 ($\phi = 28$ mm, thickness of 1.95 mm), was supplied by Gospel. The Yb^{3+} concentration in the disk was calculated from the absorption spectra to be 8.5 at.%. Both laser crystals had flat/flat surfaces, where the laser rod was HT/HR @ 940/1030 nm, respectively, on the pump side and AR @1030 nm on the other side, and the disk had an AR/AR coating @ 1030 nm on both sides.

The experimental parameters of all the Yb:YAG samples used are presented in Table 2. The pumping transition peak at 940 nm is utilized for diode pumping using InGaAs diode arrays, which are more robust than the AlGaAs diodes used to pump the Nd:YAG at 808 nm. The Yb:YAG laser crystals were longitudinally pumped by two types of conductively cooled fiber coupled diode array lasers. The first one, an OPC-B030-940-FC, with a nominal maximum fiber diameter of 1.55 mm, NA of 0.22 and an output power of 30 W, and a second diode model OPC-D060-940-FC, 1.5 mm, 0.1 NA, with a nominal output power of 60 W. The diode laser emission was centered at 940 nm at normal operating temperature of 20 °C with an emission spectral bandwidth (full width at half maximum, FWHM) of less than 4 nm. The temperature and hence the wavelength of the pumping diode were regulated by a chiller (Neslab-CFT-33). The pump radiation was collimated and focused on the front surface of the crystal with a focusing lens (OPC-ORU-03) to

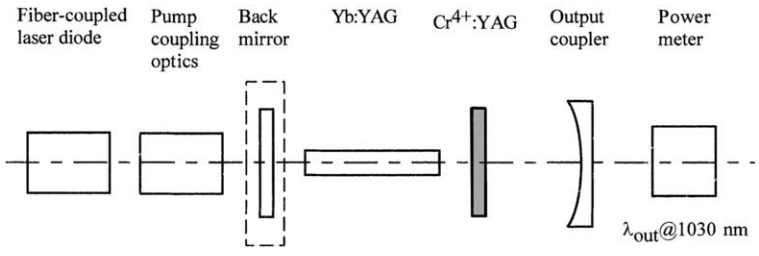

Fig. 1. Schematic of the passively Q-switched diode pumped Yb:YAG laser set-up.

Table 2
Experimental parameters of Yb:YAG crystals used in this paper

Sample	Concentration of Yb, at.%	Dimension (diameter × length, mm)	Coating	Manufacturer
#1	10	2 × 4	S1: HT/HR @ 940/1030 nm S2: AR @ 1030 nm	VLOC, FL, USA
#2	8.5	28 × 1.95	AR/AR @ 1030 nm	GOT, PR China
#3	5	2 × 4	S1: HT/HR @ 940/1030 nm	Shanghai, PR China
	10	2 × 3	S2: AR @ 1030 nm	
#4	10	15 × 1	S1: HT/HR @ 940/1030 nm	Shanghai, PR China
	20	15 × 0.5	S2: AR @ 1030 nm	
	30	15 × 0.3		
#5	10	10 × 2	AR/AR @ 1030 nm	FEE, GmbH Germany
	12	10 × 2		
	15.7	10 × 2		

obtain 627 μm beam diameter. The Yb:YAG crystalline rod was inserted inside a water-cooled copper block heat sink, whose temperature was controlled by a thermoelectric re-circulating solid-state chiller (Melcor MLA 270). In order to obtain a good thermal contact between the crystal and the heat sink, the Yb:YAG crystal was wrapped by a thin (0.1 mm) indium foil and then attached to the copper heat sink.

In the case of the Yb-crystal disk, it was sandwiched between a water-cooled, ring-shaped, circular heat sink and a copper ring (5 mm aperture). The copper ring pressed the disk against an indium foil, to achieve a good thermal contact of the crystal disk surface to the copper heat sink unit. We assume that the heat sink and the crystal surface are always in thermal equilibrium.

The laser resonator consisted of an output coupler mirror with radius of curvature, ROC = 150 mm, with various reflectivities ranging from $R = 85\%$ to 98% @ 1030–1060 nm. A front flat mirror, with high transmission coating at 940 nm and high-reflectivity (HR) coating at 1030 nm, was utilized with the disk crystal. The length of the disk and rod laser cavities, was $l_c = 52$ mm, which yielded thermally undistorted waist $\omega_c \approx 150$ μm, where ω_c is the radius $(1/e^2)$ of the fundamental mode size on the back mirror. This length accounts for the thermal lensing which results from the high pumping power densities when the laser is pumped at 300 K, and which affects the laser performance and its beam quality.

For the CW operating mode, we used an Ophir power meter, (Ophir 30A-SH) to monitor the output power.

For the pulsed passively Q-switched operation, we have inserted inside the cavity, perpendicular to the optical axis one of the crystalline samples either Cr^{4+}:YAG, Cr^{4+}:LuAG ($Lu_3Al_5O_{12}$), or Cr^{4+}:GSGG, all with nominal concentration of the chromium ion in the range 0.15–0.3 at.%. The Cr^{4+}:YAG, Cr^{4+}:LuAG samples were kindly supplied by Dr. M. Kokta of Bicron Crystals Products (USA), and that of Cr^{4+}:GSGG by Dr. Igor Ivanov, of the Research of Material Science and Technology (Russia). Some important experimental parameters [1,6] of the Cr^{4+} doped saturable absorbers used in these experiments are presented in Table 3. The Q-switch crystal surfaces were polished, without coating, and therefore their transmission spectra are accounted for Fresnel losses.

The Q-switched output laser signal was detected by a fast silicon photodiode (risetime <1 ns, collected by a digital oscilloscope (Tektronix TDS 724A), and further analyzed by commercial data processing software. For laser pulse frequency measurements, a detector with a slower risetime (3.5–18 μs) was employed, followed by an FFT analysis.

Table 3
Physical and optical parameters of Cr^{4+}:YAG samples used as saturable absorbers in diode-pumped Yb:YAG laser

Cr^{4+}:YAG parameters	Cr^{4+}:YAG (a)	Cr^{4+}:YAG (b)	Cr^{4+}:LuAG	Cr^{4+}:GSGG
l_a (mm)	0.85	0.94	1.43	0.2
α (cm^{-1})	1.32	0.28	2.9	8
T_0 (%)	89	97	66	85
Concentration Cr^{4+} (10^{17} ion/cm^3)	4.12	0.87	26.4	13.8
σ_{gsa} (10^{18} cm^2) @ 1.06 μm	3.2 [1]	3.2 [1]	1.1 [1]	5.9 [22]
σ_{esa} (10^{18} cm^2) @ 1.06 μm	0.45 [1]	0.45 [1]	0.043 [1]	0.9 [22]

The thickness of the sample is l, α is the absorption coefficient, and T_0 is the small signal transmission.

3. Results

3.1. Passively Q-switched operation—results and optimization

3.1.1. Disk configuration (sample #2)

3.1.1.1. Medium pump power level (up to 30 W). We passively Q-switched several Yb:YAG laser disks with two uncooled, polished Cr^{4+}:YAG samples denoted by (a) and (b). See Table 3 for details. In these experiments an output coupling mirror with a reflectivity of $R = 95\%$ was used. Also, in the first set of Q-switching experiments we limited the input pumping power (p_{in}) to levels of up to $P_{in} \approx 35$ W.

The Q-switched Yb:YAG (8.5 at.%) laser performance produced about 650 mW average output power at 30 W input pumping power. At this pumping level, the Q-switching element surface was damaged and the laser performance degraded by 50%. The pulsewidth, τ (denoted by the FWHM), was of the value $\tau \approx 30$ ns both at low and maximum input pumping power, for samples (a) and (b) of the saturable absorbers.

For Yb:YAG disk laser with the saturable absorber sample (a), the modulation frequency of the 1030–1048 nm laser emission varied from $f \approx 4$ to 12 kHz at input pumping levels of $P_{in} = 21$ and $P_{in} = 31$ W, respectively. Although there are slight differences between the two samples of the saturable absorbers, we cannot draw any comparative conclusions pertaining their quality as passive Q-switches, since the Cr^{4+} samples were not fabricated similarly.

Q-switching operation was applied to Yb-disk geometry with Yb^{3+} concentrations: $C_{Yb} = 10$, 12, and 15.7 at.%. The saturable absorbers used in these cases was sample (a) (e.g. $l_a = 0.85$ mm). The average output power for the 10 and 12 at.% was in the hundreds of mW, in the pumping range of 26–37 W. The pulsewidths (FWHM) in this pumping power regime were 46 and 34 ns and the modulation frequency of 4.6 and 5.65 kHz, respectively. We did not test the disk with $C_{Yb} = 15.7$ at.% for passive Q-switching due to poor free running laser performance especially above $P_{in} = 40$ W. This will be discussed further in Section 3.3.

3.1.1.2. High pump power level (up to 60 W). We tested both Yb:YAG rod (as will be described in the following section) and Yb:YAG disk for Q-switching under higher pumping load. For that purpose we used a fiber coupled diode array of 60 W output power at 940 nm. The optimal output coupling of the laser resonator was $R = 85\%$, and the Cr^{4+}:YAG was sample (a). The performance of both Yb:YAG rod and disk was degraded due to damage at the Cr^{4+}:YAG surface. When the passively Q-switched Yb:YAG disk (28×1.95 mm) was pumped in the range of 20–51 W, it produced an average output power of 3 W at 31 W pumping power. At that point the performance was degraded and the system was realigned, which resulted-in 4.2 W average output power @ 51 W pumping power.

In a separate experiment at $P_{in} = 51.8$ W, using saturable absorber samples (a) and (b) we obtained pulses of temporal widths of 43.4 and 54.4 ns (FWHM), respectively, and modulation frequency of 9.6 and 16 kHz, respectively. All these measurements were carried out using output coupling

reflectivity of $R = 95\%$ and keeping the laser crystal at $T_{crystal} = 18$ °C.

3.1.2. Laser rod configuration (sample #1)

3.1.2.1. Low pump power level (up to 30 W). Operating passively Q-switched Yb:YAG laser rod for both Cr^{4+} samples (a) and (b) at 30 W pumping power, produced pulses having temporal pulsewidth (FWHM) of $\tau \approx 16$ ns, at an average modulation frequency of $f \approx 4$ kHz. The average output power of Yb:YAG laser rod was lower than the disk geometry, namely $P_{out} \approx 100$ mW, due to damage to the Q-switching surface. Significant improvement in the Q-switched laser performance was obtained using an output coupler with a reflectivity of $R = 85\%$. We obtained maximum average output power of 1.32 W, with a slope efficiency of $\eta_{se} = 12.8\%$. For the 1.32 W average output power (@ 31 W input pumping power), the modulation frequency was $f \approx 13$ kHz, with an average pulsewidth of 22 ns. This implies that the pulse energy is ≈100 μJ/pulse and the peak power is ≈4.5 kW. At present the results with $R = 85\%$ are preliminary and no attempt was made to optimize the Q-switched performance with other output couplers. All the Q-switched measurements were performed with Cr^{4+}:YAG sample (a). The maximum error in the pulsewidth measurements is in the range of ±10%. The free running average output power was $P_{out} = 5.3$ W under the same experimental conditions of pumping power and output coupling reflectivity, (31 W, $T_{heat\ sink} = T_{crystal} = 15$ °C, and $R = 85\%$, respectively). The fraction of the Q-switched power relative to the free-running output power is defined by $\eta_{extract} = 25 \pm 0.5\%$, under the same experimental conditions. We should note here that due to the surface damage on the Q-switching element and consequently, the output power degradation at about $P_{in} \approx 26$–30 W, the pumping power did not exceed this value.

3.1.2.2. High pump power level (up to 60 W). We also tested for Q-switching the laser rod (2×4 mm) using Cr^{4+}:YAG sample (a) under higher pumping load similarly to what have been performed with Yb:YAG disk. The output coupler used was also $R = 85\%$. At input pumping power of $P_{in} = 28$ W we observed damage to the saturable absorber and degradation in the performance by ≈25%. The maximum average output power after realignment was $P_{out} = 4.2$ W @ $P_{in} = 43.5$ W input power and the curve was slightly saturated. In the pumping range of 20–51 W, the pulsewidths ranged from 48 to 38 ns, respectively, and the laser pulse frequency varied from 2 to 23.4 kHz, respectively.

To improve the Q-switching performance, we placed the Cr^{4+}:YAG inside a water cooled heat sink at 15 °C. In this configuration ($R = 85\%$), the maximum average output power was $P_{out} = 4.5$ W at an input pumping power of $P_{in} = 32.5$ W. Further increase in the pumping power, up to 53 W, led to saturation with maximum average output power, namely, $P_{out} \approx 4.8$ W. Under the same experimental conditions, the free-running output power was ≈16 W, therefore the extraction efficiency is $\eta_{extract} \approx 30\%$. The dependence of the Q-switched pulsewidth and the modulation frequency on the input pumping power is presented in Fig. 2. From this figure we observe that in the pumping range of 16–33 W, the repetition rate changed significantly from 1.2 to 9.2 kHz, respectively. The change in the pulsewidth in this range was from 54.3 to 48 ns, respectively. This configuration yields pulse energy of 0.5 mJ/pulse and peak power of ≈10.4 kW.

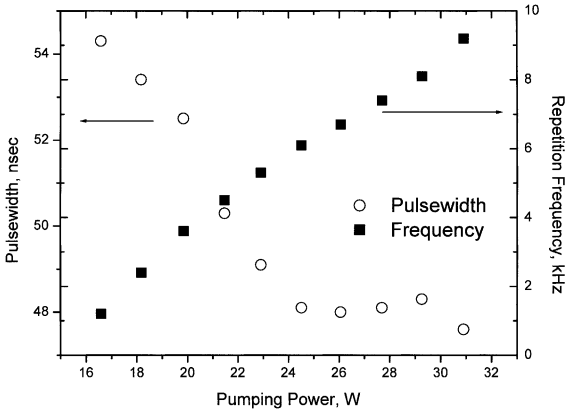

Fig. 2. The repetition frequency and output pulsewidths versus pumping power of a passively Q-switched, diode-pumped Yb:YAG/Cr^{4+}:YAG. The output coupling reflectivity is $R = 85\%$.

Finally, we used the relatively high peak power to obtain frequency doubling at 525 nm by using KTP or BBO nonlinear crystals. Both crystals generated a modulated green light with a repetition rate in the kHz frequency regime, with pulsewidths of about 20–40 ns (FWHM). At present, the output power of the green laser emission is low due to the optical system, which is not optimized for SHG operation.

3.2. Passive Q-switching with Cr^{4+}:LuAG and Cr^{4+}:GSGG

We have conducted preliminary experiments with two additional saturable absorbers based on Cr^{4+}-doped garnets. For these preliminary testing we used Yb:YAG disk (sample #1) with Yb^{3+} doping of 8.5 and 10 at.% The optimal output couplers used in all the experiments were of $R_{out} = 99\%$ and 85% for both Cr^{4+}:LuAG and Cr^{4+}:GSGG, respectively. The Cr^{4+}:LuAG and Cr^{4+}:GSGG were polished, uncoated, with small signal transmission of $T_0 \approx 66\%$ and 85%, respectively. The Cr^{4+}:LuAG is of special interest due to its highest ratio of $\sigma_{gsa}/\sigma_{esa}$ values relative to other garnets, where σ_{gsa} and σ_{esa} are the ground state and the excited state absorption cross-sections, respectively [1].

Both Cr^{4+}:LuAG and Cr^{4+}:GSGG produced much lower average output power relative to Cr^{4+}:YAG when operated as saturable absorbers for Yb:YAG laser. With Cr^{4+}:LuAG ($l = 1.43$ mm), we obtained an average output power of $P_{out} \approx 235$ mW, at $P_{in} \approx 46$ W. The modulation frequency in the pumping range 30–46 W changed from $f \approx 0.6$ to 1.7 kHz, respectively. The pulsewidth (FWHM) exhibited a small change namely, $\tau \approx 26.2$ to 24.7 ns, which is within the experimental error. For the Cr^{4+}:GSGG ($l = 0.2$ mm), we obtained average output power of $P_{out} \approx 220$ mW, with $f \approx 2.7$ kHz and $\tau \approx 16$ ns at $P_{in} \approx 60$ W.

3.3. Free-running performance

In order to characterize the working parameters and optimal conditions for passively Q-switched ytterbium laser, free-running operation mode has been studied extensively, as well. The free-running mode was operated first, in order to characterize the working parameters and optimal conditions for an efficient passive Q-switching operation of Yb:YAG laser (using samples #1 and #2), in two different geometries and at several heat sink temperatures, ranging from 5 to 20 °C. The diode-pumped Yb:YAG laser performance for Yb:YAG rod and disk at 15 °C is presented in Fig. 3(a). Since the experimental results at different temperatures behave similarly, we present only the performance at 15 °C. The Yb concentration in the rod used is $C_{Yb} = 10$ at.% ($\phi = 2$ mm, $l = 4$ mm)

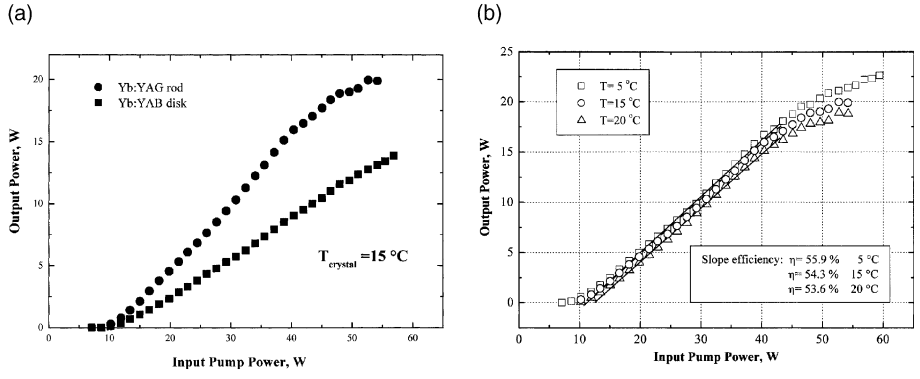

Fig. 3. (a) Laser output power of a free-running CW Yb:YAG laser rod ($C_{Yb} = 10$ at.%) and disk ($C_{Yb} = 8.5$ at.%) versus incident pumping power at 940 nm, at heat sink temperature of 15 °C. (b) Laser output power of a free-running CW Yb:YAG laser rod ($C_{Yb} = 10$ at.%) versus incident pumping power at 940 nm, at different heat sink temperatures. The various slope efficiencies are indicated in the figure.

and for the disk 8.5 at.%. (The cavity characteristics of this set-up were similar to previous experiments, namely, cavity length of 52 mm, output coupling mirror of ROC = 150 mm and a reflectivity of $R = 95\%$.) Thermal gradients result in thermal lensing and efficiency reduction due to the high temperature and subsequently, an increase in the lower Stark level population of the terminal lasing level. In order to minimize the thermal load on the crystal we reduced the radial temperature gradients by employing a disk shaped geometry for the laser medium. In this geometry, the thermal gradients are collinear with the laser beam and the axial heat removal is easier due the thinner dimension of the disk. In the case of the disk configuration, the laser output power showed linear dependence on the incident input power at same heat sink temperature range, while the laser rod performance deviated from linearity.

The slope efficiency, η_{se}, was calculated from the linear dependence of the output power on the pumping power according to

$$P_{out} = \eta_{se}(P_{in} - P_{th}),$$

where P_{out} is the laser output power, P_{in} is the input pumping power and P_{th} is the extrapolated threshold power. The maximum output power obtained at an operating temperature of $T_{heat\ sink} = T_{crystal} = 5$ °C in the above pumping scheme is $P_{out} = 22.2$ W, with a slope efficiency of $\eta_{se} = 56\%$. When the crystal temperature was increased up to 20 °C, the Yb:YAG output power degraded slightly to $P_{out} = 19$ W, with a slope efficiency, $\eta_{se} = 53.6\%$. The free-running performance of Yb:YAG rod at different operating temperatures is presented in Fig. 3(b). In all the experiments, the laser was pumped around the maximum absorption peak (941 nm), where most of the pump light was absorbed. The temperature effects on the laser performance are clearly observed at high pumping load, where deviation from linear fitting in the input–output curves are observed. The radial temperature gradient inside the laser rod (relative to the heat sink temperature) was calculated using the formula of Innocenzi et al. [7]. In the rod center $r = 0$, the relative temperature, $T(r = 0)$ was calculated as 140 °C, while at the crystal surface, namely, at $r = r_0 = 1$ mm, the temperature was calculated to be $T(r = r_0) = 15$ °C. This performance is similar (although different in beam quality) to the results of Giesen et al. [8] for Yb(8 at.%):YAG, under similar pump power level, and at ambient temperature. Under these experimental conditions, Giesen et al. obtained free-running output power of about 18 W by using a thin disk laser (0.3 mm thickness) with four double-passes of the pump light. Furthermore, improvement in the output power and in the total optical efficiency were obtained by Karszewski et al. [9] (to values of 47–45%), in the same temperature range, however, with eightfold passes of the pumping light through the crystal. Our total optical efficiencies at 54 W pumping input power (single-pass) obtained at heat sink temperatures of, $T = 5$, 10, and 20 °C, are 39%, 36.6%, and 34.7%, respectively.

The beam quality factor, M^2, of Yb:YAG was measured in both the rod and disk geometries. The values of M^2 yield further indication as to the influence of the thermal gradients on the laser performance. The beam quality was measured by using the knife-edge technique. The beam size $D(z)$ was measured between 13.5% and 86.5% clip-level [10]. The measured values of $D(z)$ were fitted to the propagation equation:

$$D^2(z) = D_0^2 + 4\theta^2(z - z_0)^2,$$

where D_0 is the width of the beam waist located at a position z_0, and θ is the divergence angle. By using these parameters, the values of M^2 were calculated by

$$M^2 = \frac{\pi D_0 \theta}{2\lambda},$$

where λ is the laser wavelength. For Yb:YAG rod ($C_{Yb} = 10$ at.%) and Yb:YAG disk ($C_{Yb} = 8.5$ at.%), the beam quality factors at 53 W input power are 3.15 and 2.51, respectively. This confirms our assumption of better thermal management in the disk geometry.

3.4. Concentration dependence

The concentration of Yb^{3+} active ion is a crucial factor in the proper performance of Yb laser. This stems from the quasi-three level nature of ytterbium laser and the reabsorption of the laser

emission. We tested several samples of Yb:YAG with different doping levels in order to establish a relationship between the laser performance and the active ion concentration. All the experiments were performed at crystal heat sink temperature, $T_{\text{heat sink}} \approx T_{\text{crystal}} = 16$ °C. The lengths of the 5 and 10 at.% laser rods were adjusted for ≈87% and ≈95% absorption of the pumping power, respectively. The laser performance tests for samples #3 and #4 were made on samples from the same vendor and under the same experimental conditions, which implies similar growth and coating conditions. By using set samples #3 of Yb:YAG rods with $C_{\text{Yb}} = 10$ and 5 at.%, we obtained slope efficiencies of 37% and 25.5%, respectively. The results were recorded for a variety of output couplers, ranging from $R = 92\%$ to 99% (at $T_{\text{crystal}} = 16$ °C). We also used a mechanical chopper (duty cycle of 50%) to minimize thermal effects and possible damage to the crystals. For the laser rods with $C_{\text{Yb}} = 10$ and 5 at.%, the laser performed best with output coupler of $R = 95\%$. For $C_{\text{Yb}} = 5$ at.% we observed a variation of ≈20% in the maximum output power among different samples from the same boule. Also we noticed instabilities in the output power above 20 W absorbed power, probably due to thermal effects inside the Yb:YAG crystal. We should note here the effect of pumping wavelength variation with the diode current on the Yb laser performance, for both $C_{\text{Yb}} = 10$ and 5 at.% While the optimal wavelength at the maximum current is $\lambda = 942$ nm, there is a significant blue shift at lower diode currents, and this affects the amount of the absorbed power. With the $C_{\text{Yb}} = 10$ at.% the instabilities of output power with time were much higher and in some cases led to 20% degradation of the initial power after 25 min of CW operation.

We should mention here that unlike other reports, no lasing action was observed under the same experimental conditions and at ambient temperature with samples #4, namely, $C_{\text{Yb}} = 20$ and 30 at.% (set samples #4), either when pumped at the absorption peak (941 nm) or at the shoulder of the absorption (935 nm). This is attributed to the strong ground state re-absorption at the lasing wavelength. All the samples were of disk shape and adjusted for 60–63% absorption at 941 nm. Only the 10 at.% samples of this set performed similarly to Yb:YAG rod (samples #3), in the output coupling range of $R = 99$–95%, and with slope efficiency of $\eta_{\text{se}} = 38\%$.

3.5. Losses and gain in Yb:YAG system

The total round-trip losses in the Yb:YAG laser system were estimated by using the Findlay–Clay method. This is done by measuring the various pumping input power at threshold versus the output coupling mirror reflectivities [11]. The following equation provides the relation between the two parameters:

$$-\ln(R) = 2KP_{\text{th}} - L, \tag{1}$$

where R is the reflectivity of the output mirror, and K is the pumping coefficient defined as the product of all the coefficients that lead to the population of the upper lasing state. Eq. (1) is valid for only a four-level system. We use it for Yb^{3+} assuming that under proper thermal management the system is a quasi-three-level. This point, will be verified later in the text. The incident pumping power at threshold is defined by P_{th}, and L represents the total round-trip losses, defined as: $L = 2\delta l + L_{\text{M}}$. Here, l is the crystal length, and δ are the passive losses per unit length. The value of L_{M} represents various losses [12], such as absorption or scattering losses at the back (HR) mirror, or diffraction losses of the resonator and is estimated as $L_{\text{M}} \approx 1\%$. The laser was operated for optimal performance using different output coupler reflectivities ranging from 85% to 98%. The best performance obtained for both the Yb:YAG rod and the disk (samples #1 and #2) were at $R = 95\%$. The values of L and K can be extracted from the linear plot of $-\ln(R)$ vs. P_{th} according to Eq. (1). The values for the total round-trip losses are, $L = 8\%$ and the factor $K = 6.725 \times 10^{-3}$ W^{-1} for 10 at.% ytterbium laser rod. For the 8.5 at.% Yb^{3+} laser disk, the total round trip losses are, $L = 9.3\%$, and the factor K is, $K = 7.15 \times 10^{-3}$ W^{-1}. The experimental measurement error is ±10%. The passive losses per unit length extracted from our results (assuming that $L_{\text{M}} \approx 1\%$) are 8.75% and 21% per cm for the ytterbium laser rod and disk laser, respectively.

The small signal gain at threshold is calculated from the following formula:

$$g_{\mathrm{th}} = \frac{KP_{\mathrm{th}}}{l}. \tag{2}$$

From this expression, the small signal gain at threshold (with 95% reflectivity of the output coupler) is obtained: $g_{\mathrm{th}}(\text{Yb-rod}) \approx 0.132\ \mathrm{cm}^{-1}$ and $g_{\mathrm{th}}(\text{Yb-disk}) \approx 0.4\ \mathrm{cm}^{-1}$. From the values of gain at threshold and the known values of stimulated emission cross-section, the population inversion at threshold can be estimated using the following relationship:

$$\begin{aligned} g_{\mathrm{th}} &= \sigma_{\mathrm{em}} N_{2\mathrm{th}} - \sigma_{\mathrm{ab}} N_{1\mathrm{th}} \\ &= \sigma_{\mathrm{em}} N_{2(j=1)\mathrm{th}} - \sigma_{\mathrm{ab}} N_{1(j=3)\mathrm{th}}, \end{aligned} \tag{3}$$

where $N_{2\mathrm{th}} = N_{2(j=1)\mathrm{th}}$ is the lowest Stark component, $j = 1$, of the excited state ($^2F_{5/2}$) population density at threshold, N_2, and $N_{1\mathrm{th}} = N_{1(j=3)\mathrm{th}}$ is $j = 3$ Stark component of the ground state ($^2F_{7/2}$) population density at threshold, N_1, located at 612 cm^{-1} above the ground state. The stimulated emission cross-section at 1030 nm, σ_{em}, has the value of: $\sigma_{\mathrm{em}} = 2.3 \times 10^{-20}\ \mathrm{cm}^2$ [13]. We assume that at threshold, the ground state population depletion due to ground state absorption is small, e.g. $N_1 \ll N_{\mathrm{T}}$ (N_1 is the ground state ion density and N_{T} is the total ion density). Therefore, at threshold we have that

$$\sigma_{\mathrm{em}} N_{2(j=1)\mathrm{th}} \gg \sigma_{\mathrm{ab}} N_{1(j=3)\mathrm{th}}, \tag{3a}$$

and it follows that gain at threshold is given by

$$g_{\mathrm{th}} \approx \sigma_{\mathrm{em}} N_{2(j=1)\mathrm{th}} = \sigma_{\mathrm{em}} \Delta N_{\mathrm{th}}, \tag{3b}$$

where ΔN_{th} is the population inversion at threshold. The values obtained for ΔN_{th} are therefore 5.7×10^{18} and $1.74 \times 10^{19}\ \mathrm{cm}^{-3}$, for Yb:YAG rod and disk, respectively. The differences in gain, losses, and hence, in the population inversion at threshold are attributed the different crystal quality and the presence of impurities which are present in small amounts in the Yb:YAG samples and which contributes to degradation in laser performance [14].

4. Summary and conclusions

In the present paper, we report the results of optimizing the working parameters of an efficient operation of a microlaser, based on a passive Q-switched diode-pumped Yb:YAG laser. The resonator optimization accounts for the thermal lensing which results from the high pumping power densities when the laser is pumped at 300 K, and which affects the laser performance and its beam quality.

The usefulness of tetravalent chromium-doped garnets as saturable absorbers is demonstrated by achieving repetitive modulation of a CW Yb:YAG laser operation. By using Yb:YAG/Cr^{4+}:YAG crystals, it produces modulated light in the kHz frequency range with pulsewidths in the 16–48 ns temporal regime. Maximum peak power of 10.4 kW, at an average output power of 4.5 W, is reported. The optimization yields extraction of Q-switched pulses of ≈0.5 mJ/pulse, with extraction efficiency of ≈30% relative to the free-running mode under the same experimental conditions. Our experimental results of average output power, modulation frequency, and pulsewidth in Yb:YAG/Cr^{4+}:YAG system are in agreement with the recent results of Patel and Beach [15]. The performance of Cr^{4+}:YAG as a saturable absorber is superior relative to that of Cr^{4+}:LuAG or Cr^{4+}:GSGG. By utilizing the significant advantages of Yb^{3+} ion, we are currently developing a compact diode-pumped Yb:YAG microlaser.

Acknowledgements

This work was supported by the "MAGNET" program of the Chief Scientist Office at the Israeli Ministry of Industry and Trade, Consortium of Diode Pumped Solid State Lasers (LESHED).

References

[1] Y. Kalisky, A. Ben Amar-Baranga, Y. Shimony, M.R. Kokta, Opt. Mater. 8 (1997) 129.

[2] K.S. Bagdasarov, G.A. Bogomolova, D.N. Vylegzhanin, A.A. Kaminskii, A.M. Kevorkov, A.M. Prokhorov, Sov. Phys. Dokl. 19 (6) (1974) 358.
[3] T.Y. Fan, IEEE J. Quant. Electron. 29 (1993) 1457.
[4] A. Giesen, H. Hugel, A. Voss, K. Wittig, U. Brauch, H. Opower, Appl. Phys. B 58 (1994) 365.
[5] J. Aus der Au, G.J. Spuhler, T. Sudmeyer, R. Paschotta, R. Hovel, M. Moser, S. Erhard, M. Karszewski, A. Giesen, U. Keller, Opt. Lett. 25 (2000) 859.
[6] Z. Burshtein, P. Blau, Y. Kalisky, Y. Shimony, M. Kokta, IEEE J. Quant. Electron. 34 (1998) 292.
[7] M.E. Innocenzi, H.T. Yura, C.L. Fincher, R.A. Fields, Appl. Phys. Lett. 56 (19) (1990) 1831.
[8] A. Giesen, U. Brauch, I. Johannsen, M. Karszewski, C. Stewen, A. Voss, High-power near diffraction-limited and single-frequency operation of Yb:YAG thin disk laser, in: S.A. Scheps, C. Pollock (Eds.), OSA Trends in Optics and Photonics on Advanced Solid State Lasers, vol. 1, Optical Society of America, Washington, DC, 1996, pp. 11–13.
[9] M. Karszewski, U. Brauch, K. Contag, S. Erhard, A. Giesen, I. Johannsen, C. Stewen, A. Voss, 100-w TEM_{00} operation of Yb:YAG thin disk laser with high efficiency, in: S.A. Scheps, C. Pollock (Eds.), OSA Trends in Optics and Photonics, vol. 19, Advanced Solid State Lasers, Optical Society of America, Washington, DC, 1996, pp. 296–299.
[10] A.E. Siegman, M.W. Sansett, T.F. Johnston, IEEE J. Quant. Electron. 27 (1991) 1098.
[11] D. Findlay, R.A. Clay, Phys. Lett. 20 (1966) 277.
[12] W. Koechner, Solid State Laser Engineering, fifth ed., Springer-Verlag, 1999.
[13] H.W. Bruesselbach, D.S. Sumida, R.A. Reeder, R.W. Byren, IEEE. J. Quant. Electron. 3 (1) (1997) 105.
[14] P. Le Boulanger, S. Levy, Z. Burshtein, Y. Kalisky, S.R. Rotman, P. Deng, H. Yin, W. Chen, F. Gan, Spectroscopic properties of Yb^{3+}-doped silicate and fluorophosphate glasses, private communication.
[15] F.D. Patel, R.J. Beach, IEEE. J. Quant. Electron. 37 (2001) 707.
[16] R.J. Beach, Opt. Commun. 123 (1995) 385.
[17] L.D. DeLoach, S.A. Payne, L.L. Chase, L.K. Smith, W.L. Kway, W.F. Krupke, IEEE J. Quant. Electron. 29 (1993) 1179.
[18] V.V. Ter-Mikirtychev, V.A. Fromzel, Appl. Opt. 39 (27) (2000) 4964.
[19] S.A. Payne, L.K. Smith, L.D. DeLoach, W.L. Kway, J.B. Tassano, W.F. Krupke, IEEE. J. Quant. Electron. 30 (1994) 170.
[20] D.C. Brown, IEEE. J. Quant. Electron. 33 (1997) 861.
[21] D.S. Sumida, T.Y. Fan, Opt. Lett. 19 (17) (1994) 1343.
[22] M.I. Demchuk, N.V. Kuleshov, V.P. Mikahailov, IEEE. J. Quant. Electron. 30 (1994) 2120.